CO$_2$ Transport, Variability, and Budget over the Southern California Air Basin Using the High-Resolution WRF-VPRM Model during the CalNex 2010 Campaign✐

CHANGHYOUN PARK,[a] CHRISTOPH GERBIG,[b] SALLY NEWMAN,[c] RAVAN AHMADOV,[d] SHA FENG,[e]
KEVIN R. GURNEY,[f] GREGORY R. CARMICHAEL,[g] SOON-YOUNG PARK,[h] HWA-WOON LEE,[h]
MIKE GOULDEN,[i] JOCHEN STUTZ,[j] JEFF PEISCHL,[k] AND TOM RYERSON[k]

[a] *Institute of Environmental Studies, Pusan National University, Busan, South Korea*
[b] *Max Plank Institute for Biogeochemistry, Jena, Germany*
[c] *Division of Geological and Planetary Sciences, California Institute of Technology, Pasadena, California*
[d] *Model Development Branch, Global Systems Division, Earth System Research Laboratory, National Oceanic and Atmospheric Administration, Boulder, Colorado*
[e] *Department of Meteorology and Atmospheric Sciences, The Pennsylvania State University, University Park, Pennsylvania*
[f] *School of Life Sciences, Arizona State University, Tempe, Arizona*
[g] *Center for Global and Regional Environmental Research, Iowa City, Iowa*
[h] *Department of Atmospheric Environmental Sciences, Pusan National University, Busan, South Korea*
[i] *Department of Earth System Science, University of California, Irvine, Irvine, California*
[j] *Department of Atmospheric and Oceanic Sciences, University of California, Los Angeles, Los Angeles, California*
[k] *Chemical Sciences Division, Earth System Research Laboratory, National Oceanic and Atmospheric Administration, Boulder, Colorado*

ABSTRACT

To study regional-scale carbon dioxide (CO$_2$) transport, temporal variability, and budget over the Southern California Air Basin (SoCAB) during the California Research at the Nexus of Air Quality and Climate Change (CalNex) 2010 campaign period, a model that couples the Weather Research and Forecasting (WRF) Model with the Vegetation Photosynthesis and Respiration Model (VPRM) has been used. Our numerical simulations use anthropogenic CO$_2$ emissions of the Hestia Project 2010 fossil-fuel CO$_2$ emissions data products along with optimized VPRM parameters at "FLUXNET" sites, for biospheric CO$_2$ fluxes over SoCAB. The simulated meteorological conditions have been validated with ground and aircraft observations, as well as with background CO$_2$ concentrations from the coastal Palos Verdes site. The model captures the temporal pattern of CO$_2$ concentrations at the ground site at the California Institute of Technology in Pasadena, but it overestimates the magnitude in early daytime. Analysis of CO$_2$ by wind directions reveals the overestimate is due to advection from the south and southwest, where downtown Los Angeles is located. The model also captures the vertical profile of CO$_2$ concentrations along with the flight tracks. The optimized VPRM parameters have significantly improved simulated net ecosystem exchange at each vegetation-class site and thus the regional CO$_2$ budget. The total biospheric contribution ranges approximately from −24% to −20% (daytime) of the total anthropogenic CO$_2$ emissions during the study period.

1. Introduction

It is well known that carbon-induced global warming by human activities that use fossil-fuel combustion has become a serious issue for climate change. About 30%–40% of anthropogenic greenhouse gases (GHGs) are emitted from urban areas (Seto et al. 2014), and these emissions are associated with an increase of average temperature, higher intensity and occurrence of severe weather, and an increase and/or decrease of precipitation (IPCC et al. 2013). Given its high concentration and emissions, carbon dioxide (CO$_2$) is the GHG most in need of monitoring, despite its lower global warming potential (GWP) relative to some other GHGs (e.g., methane, nitrous oxide, and sulfur hexafluoride respectively have 25, 298, and 22 800 times

Corresponding author: Changhyoun Park, chpark@live.com

the GWP of CO_2 over a 100-yr time horizon; Forster et al. 2007).

To understand better the effect of all emissions of CO_2 on the atmospheric carbon cycle, a wide variety of studies have been carried out using both bottom-up and top-down approaches. In the bottom-up approach, inventory statistics of fossil-fuel consumption from each source sector, including the residential, commercial, industrial, and transportation sectors, are combined with estimates of CO_2 emissions with carbon contents of each fuel type. From this approach, estimated CO_2 emissions showed an uncertainty of approximately ±5% uncertainty at the global scale (Le Quere et al. 2014) and 50%–200% at the urban scale (Turnbull et al. 2011; Asefi-Najafabady et al. 2014). In contrast, the top-down approach includes atmospheric flux measurements and inversion modeling. Microscale flux-measurement studies have been conducted in vegetation-dominated areas for decades to quantify and understand the interactions between the surface and the atmosphere in the carbon budget, mainly focusing on the net ecosystem exchange (NEE) of CO_2; these studies include ''AmeriFlux'' and ''FLUXNET'' (Baldocchi et al. 2001). The accuracy of the flux measurements is generally limited by the local features of land use, emission sources, and climate, however. Global-scale inverse modeling has been carried out to retrieve NEE from observed concentrations (Gurney et al. 2009; Peylin et al. 2005; Tans et al. 1990). In addition to the fact that the lack of spatially explicit a priori flux estimates can cause large uncertainties in this approach, however, the resolution of global inverse modeling is too coarse to capture the spatiotemporal resolution of microscale flux measurements. Several studies have been conducted to diagnose the mismatch between global-scale models and flux measurements (Gerbig et al. 2003; Pérez-Landa et al. 2007; van der Molen and Dolman 2007).

To fill the scale gap between the global inverse modeling and the microscale measurements, we require modeling of regional-scale CO_2 transport with finer spatiotemporal resolution. Accurate simulations of mesoscale transport are important to estimate the CO_2 transport, variability, and budget, which can only be established with high-resolution mesoscale models that include the transport of CO_2 and the CO_2 exchange flux between the biosphere and the atmosphere. Ahmadov et al. (2007, 2009) coupled a meteorological model, the Weather Research and Forecasting (WRF) Model, with the Vegetation Photosynthesis and Respiration Model (VPRM) and conducted CO_2 modeling over Europe. The results showed significant improvement in capturing mesoscale circulations and observed CO_2 spatiotemporal variation, which had not been represented

well in global models. Pillai et al. (2011) also validated the coupled model over mountain terrain by comparing it with tall-tower measurements at Mount Ochsenkopf in Germany. Jamroensan (2013) conducted VPRM parameter optimization for the newly added vegetation classes over the U.S. Midwest and estimated the interactions between the areas growing soybeans and the atmosphere. These previous studies have been mostly conducted over vegetation-dominated and relatively heterogeneous areas. In urban areas, anthropogenic emission sources and vegetation sinks of CO_2 are complexly mixed. Despite the difficulties encountered in setting up flux-measurement platforms in city areas, urban flux-measurement studies have recently been conducted that focus on the CO_2 cycle, driven by both anthropogenic emission sources and biospheric uptake (Park and Schade 2016; Velasco et al. 2013; Kotthaus and Grimmond 2012).

In the United States, urban areas have been developing rapidly by population increase and land-use modification during the last five decades (Auch et al. 2004). The main anthropogenic CO_2 emission sources are land-use changes affecting interactions between the surface and the atmosphere and fossil-fuel combustion for energy, transportation, and industrial processes, as reported in the U.S. GHG inventory report of the Environmental Protection Agency (http://www.epa.gov/climatechange/ghgemissions/usinventoryreport.html). Carbon dioxide emissions account for approximately 82% of all U.S. GHG emissions from human activity (National Research Council 2010). California is one of the most significant carbon emitters in the United States, and there have been many efforts (including Assembly Bill 32: the ''Global Warming Solutions Act of 2006'') and reports addressing reduction of carbon emissions. The main sources of CO_2 in California are the transportation (~39%), industrial (~23%), electric-power (~19%), agricultural (~8%), residential (~6%), and commercial (~5%) sectors, according to the 2015 state energy-related CO_2-emission report of the Energy Information Administration (EIA; https://www.arb.ca.gov/cc/inventory/data/data.htm).

The Southern California Air Basin (SoCAB), designated by the state government of California in 1969 for the purpose of air-quality management in Southern California, includes all of Orange County and the nondesert regions of Los Angeles (LA), Riverside, and San Bernardino Counties. This region is bounded on the south and the west by the Pacific Ocean, on the north by the San Gabriel (3068 m) and San Bernardino (3505 m) Mountains, on the northwest by Mount Santa Susana (1142 m) and the Simi Hills (652 m), and on the east by Mount San Jacinto (3302 m) and Mount Santa Rosa

(2657 m). This topography causes unique meteorological flows in SoCAB, combining with the sea breeze that is linked with ''Catalina'' eddies. When low pressure forms over the desert in southern California and Arizona and high pressure builds over the Pacific Ocean off the coast at the same time during spring, northerlies flow down to the California coast, turning toward the coast of Southern California, interacting with the islands and the shape of the coast, and forming a center of eddies near Catalina Island, the so-called Catalina eddies. The swirling winds off the coast of Southern California transport large amounts of polluting emissions and finally accumulate them within SoCAB because the mountains block ventilation out of the basin. Thus, SoCAB shows relatively higher concentration of tracers when compared with areas outside SoCAB (Ryerson et al. 2013; Conil and Hall 2006; Ulrickson and Mass 1990). In 2010, therefore, the California Research at the Nexus of Air Quality and Climate Change (CalNex) campaign was conducted in and over LA and Sacramento to research issues related to air quality and climate change (Angevine et al. 2012).

Brioude et al. (2013) recently performed inverse modeling over SoCAB for the CalNex 2010 campaign and showed 31%–44% higher CO_2 emissions in 2010 as posterior than in 2002. Newman et al. (2013) used CO_2 ground measurements during the same study period and estimated that local fossil-fuel combustion contributed up to ~50% overnight and ~100% near midday. Feng et al. (2016) more recently conducted sensitivity studies in terms of the impact of the model frame and the fossil-fuel CO_2 emissions priors' spatial resolution [emissions from the ''Vulcan'' database at 10-km resolution vs LA emissions from the Hestia Project (Hestia-LA) at 1.3 km] on the simulated CO_2 concentration using the WRF Model coupled with a chemistry model (WRF-Chem) over the LA megacity during the CalNex 2010 period. They concluded that the higher-resolution simulation better resolved the vertical gradient of meteorological variables and that higher resolution of the fossil-fuel CO_2 emission data produced a more improved CO_2 simulation.

In this study, the method for the modeling system is similar to the study described by Feng et al. (2016), but our motivation and approach are different. First, we applied the newly updated Hestia-LA emissions data (version 2.1) combined with the Fossil Fuel Data Assimilation System (FFDAS) data and the National Oceanic and Atmospheric Administration (NOAA) CarbonTracker CO_2 mole fraction data from the ''CT2015'' release. Second, because of the significance of the parameters of photosynthesis and respiration in estimating biogenic contributions in specific regions,

we optimized the VPRM parameters with flux measurements at each representative vegetation site of FLUXNET. Third, we evaluated the model's performance by comparing with aircraft measurements as well as ground observations. Last, we estimated the regional CO_2 budget over SoCAB.

2. WRF-VPRM model

a. WRF modeling system

A diagnostic vegetation model that computes biospheric CO_2 fluxes (VPRM) is coupled to WRF-Chem (version 3.8.1) and is hereinafter referred to as WRF-VPRM. It has been described by Ahmadov et al. (2007) and Mahadevan et al. (2008).We set up and ran WRF by two-way nesting at 36-, 12-, and 4-km resolution on three nested grids (Fig. 1) and 38 vertical layers (with 12 layers below 1.5 km) extending up to 100 hPa, where the lowest scalar-level height was ~27 m. Initial and boundary conditions for meteorological fields and soil initialization fields for the WRF modeling were taken from the 3-h North American Regional Reanalysis dataset with 32-km spatial resolution (Mesinger et al. 2006). For sea surface temperature (SST) fields, the 6-h National Centers for Environmental Prediction SST dataset with 8-km horizontal resolution (ftp://polar.ncep.noaa.gov/pub/history/sst/ophi) was used. The WRF single-moment three-class microphysics scheme, the new Grell cumulus scheme (only for coarse domains), and the Rapid Radiative Transfer Model for GCMs (RRTMG) short- and longwave radiation schemes were used. For planetary boundary layer (PBL) diagnosis, we used the nonlocal PBL parameterization scheme of Yonsei University (Hong et al. 2006) with the ''topo_wind'' option, after conducting sensitivity tests of PBL schemes (for details, see the online supplementary material that accompanies this paper). This option was adopted to reduce overestimations of wind speeds, which have often appeared in previous studies (e.g., Bernardet et al. 2008; Angevine et al. 2012) and are due mainly to the unresolved orographic features producing less drag in WRF (Jimenez and Dudhia 2012). The model ran for 33 days from 0000 UTC 14 May to 0000 UTC 16 June, and each run was done for 30 h after each reinitialization, following the setup of Ahmadov et al. (2007, 2009), starting at 0000 UTC on the day, where the first 6 h were used for spinup.

b. Vegetation Photosynthesis and Respiration Model

VPRM is a simple diagnostic biospheric CO_2 flux parameterization that uses high-resolution land-use and satellite data along with simulated radiation and air
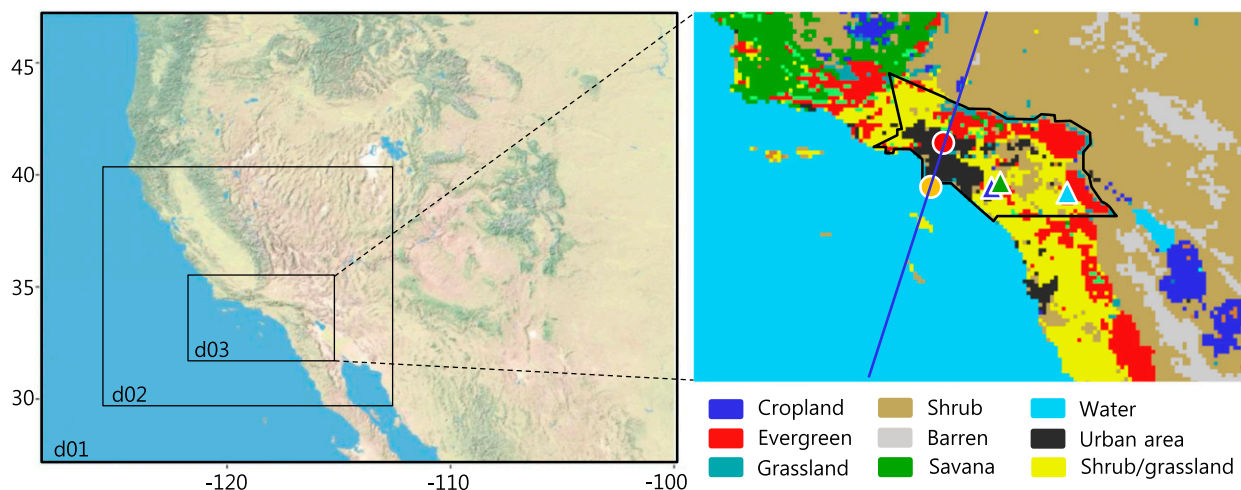
FIG. 1. (left) Domains for WRF-VPRM modeling, and (right) land-use distributions for the finest domain, with the locations of CIT (red dot), PV (orange dot), and the FLUXNET sites including coastal sage (dark-blue triangle), grassland (green triangle), and oak/pine forest (light-blue triangle). The border of SoCAB is indicated by the black boundary line. The solid blue line indicates the cross-sectional path for Fig. 4.

temperature by the WRF Model (Mahadevan et al. 2008). This enables simulation of biospheric CO_2 uptake and release fluxes at high spatiotemporal resolution. In several studies (Ahmadov et al. 2007, 2009; Pillai et al. 2011; Feng et al. 2016), the VPRM parameterization was successfully applied to different ecosystems.

VPRM derives biospheric CO_2 fluxes using flux-measurement data and MODIS (http://modis.gsfc.nasa.gov/) satellite indices, including an enhanced vegetation index and land surface water index obtained at 500-m spatial resolution with 8-day frequency. VPRM uses eight land-use categories, including evergreen forest, deciduous broadleaf forest, mixed forest, shrubland, savanna, cropland, grassland, and urban or snow/ice, that were classified on the basis of the 1-km global Synergetic Land Cover Product (SYNMAP; Jung et al. 2006). Each vegetation category has its own parameters—so-called VPRM parameters—that should be optimized on the basis of local CO_2 flux measurements for each representative land-use category.

The gross ecosystem exchange (GEE) is controlled by light, temperature, humidity, CO_2 concentration, soil moisture, nutrient availability, and seasonal leaf foliage, and the respiration is determined by autotrophs (vegetation) and heterotrophs (symbiotic microorganisms in soil) (Bowden et al. 1993; Ryan and Law 2005). In VPRM, GEE was calculated using the shortwave radiation (SWDOWN) generated by WRF combined with VPRM parameters that include the product of the maximum quantum yield λ and the half-saturation value of photosynthetically active radiation PAR_0. The respiration rate was calculated from the model's 2-m air

temperature along with first-order linear parameters including a slope α and an intercept β (Jamroensan 2013). VPRM parameters were first optimized by Mahadevan et al. (2008) through nonlinear least squares with the U.S. 1-km International Geosphere–Biosphere Programme classification (Belward et al. 1999), and then the NOAA WRF-Chem group released optimized values for U.S. vegetation as the "default" to the model's source code (Table 1). The optimization is to minimize the sum of squares of error between predicted NEEs and measured NEEs. First, the measured NEE under the condition of friction velocity $u_* \leq 0.1\,\mathrm{m\,s^{-1}}$ was removed. Then, the growing-season nighttime NEE was used to optimize α, and α was used to obtain the respiration. The measured GEE was calculated by subtracting the respiration rate from the measured NEE, and the measured GEE was used to optimize λ and PAR_0. In this approach, the intercept β is set to 0. Further details of the optimization method can be found in Mahadevan et al. (2008) and Jamroensan (2013).

c. CO₂ input data

For lateral boundary conditions and initial conditions for CO_2 concentration, we used the CT2015 dataset (ftp://aftp.cmdl.noaa.gov/products/carbontracker/co2/CT2015/molefractions/), representing the study year 2010. The CT2015 data include global background, photosynthesis/respiration by the biosphere, fires, combustion of fossil fuels, and air–sea exchange, with $1° \times 1°$ spatial resolution over all of North America up to the tropopause, with 3-h temporal resolution (Peters et al. 2007). The

TABLE 1. Optimized and default VPRM parameters under the condition of $u_* > 0.1\,\mathrm{m\,s^{-1}}$ for this study.

Vegetation class	Posterior (optimized)				Prior (default)			
	PAR_0	λ	α	β	PAR_0	λ	α	β
Evergreen	1267.0	−0.0351	0.0380	0.0	261.0	−0.2492	0.3301	0.0
Deciduous[a]	—	—	—	—	324.0	−0.1729	0.3258	0.0
Mixed forest	501.7	−0.0732	0.0703	0.0	206.0	−0.2555	0.3422	0.0
Shrubland	595.9	−0.1319	−0.0534	0.0	363.0	−0.0874	0.0239	0.0
Savanna	1297.0	−0.0301	−0.0012	0.0	682.0	−0.1141	0.0049	0.0
Cropland[a]	—	—	—	—	757.0	−0.1533	0.2680	0.0
Grassland	541.2	−0.0959	0.0378	0.0	157.0	−0.1335	0.0269	0.0
Urban area	0.0	0.0	0.0	0.0	0.0	0.0	0.0	0.0

[a] Case in which the default parameters were used when the FLUXNET site was unavailable for the vegetation class.

pressure-interfaced CT2015 pressure level was corrected to WRF pressure levels by linear interpolation, and its maximum offset was 3 hPa at ground level.

In addition to the CT2015 data, hourly fossil-fuel CO_2 emissions from the Hestia Project (version 2.1) gridded at 1.0 km for 2010 (Gurney et al. 2012; http://hestia.project.asu.edu/) were used for parallel sets of numerical experiments to feed surface boundary conditions. Because the Hestia emissions only cover SoCAB areas, emissions from outside the Hestia domain were derived from the total anthropogenic emissions from FFDAS (Asefi-Najafabady et al. 2014) and shipping and aviation emissions taken from the Emission Database for Global Atmospheric Research (EDGAR; Petrescu et al. 2012) for all three domains.

In this study, to improve performance and reduce simulation uncertainties induced by VPRM parameters, we optimized VPRM parameters for each vegetation type over Southern California, using CO_2 flux measurements at FLUXNET sites (http://www.ess.uci.edu/~california/). The sites used were the oak/pine forest site (33°48′29″N, 116°46′19″W) for evergreen forest, the pine/juniper site (33°36′18″N, 116°27′18″W) for mixed forest, the coastal sage site (33°44′02″N, 117°41′46″W) for shrubland, the desert chaparral site (33°36′36″N, 116°27′00″W) for savanna, and the grassland site (33°44′13″N, 117°41′42″W) for grassland. For the other vegetation classes not measured by FLUXNET sites, the default values were used as in the setup of Feng et al. (2016). Table 1 reports our optimized (posterior) and the default (prior) VPRM parameters.

3. Observation data

To address research issues related to air quality and climate change, the CalNex campaign was conducted in and over Los Angeles, Bakersfield, and Sacramento during May–June 2010; specific information about CalNex 2010 has been published by Ryerson et al. (2013)

and posted online by NOAA (http://www.esrl.noaa.gov/csd/calnex/). In situ continuous ground measurements were conducted on a 10-m tower at the California Institute of Technology campus (CIT; 34°08′12″N, 118°07′39″W) in Pasadena, California (Fig. 1). Meteorological variables were measured by various sensors, and the planetary boundary layer heights (PBLH) were retrieved by a Vaisala, Inc., Ceilometer CL31 model [the methods are described in Haman et al. (2012)]. Along with the measurements of chemical compounds such as aerosols and gases, CO_2 was measured by a Picarro, Inc., model G1101-i isotopic CO_2 analyzer (cavity ring-down spectroscopy). The 10-min averages of meteorological variables and the 15-min averages of PBLH measurements were integrated into the hourly averaged time series for comparison with the WRF-VPRM modeling results at each hour.

The NOAA P-3 aircraft was also instrumented to make vertical profiles of meteorological variables and chemical species. Measurement accuracies were estimated at 0.5°C for temperature, 5% for water vapor, 5° for wind direction, $1\,\mathrm{m\,s^{-1}}$ for wind speed, and 0.2 ppm for CO_2 concentration (Peischl et al. 2012).

4. Results and discussion

The WRF-VPRM model's results have been evaluated by comparison with observations during the period from 14 May to 15 June 2010. "Daytime" and "nighttime" are defined as hours from 0600 to 1900 LST and from 2000 to 0500 LST of the next day, respectively. Basic statistical measures used here are the root-mean-square error (RMSE), the mean bias (MB; simulations minus observations), and the index of agreement (IOA; Willmott 1982), and their equations can be expressed as

$$\mathrm{RMSE} = \left[\sum_{i=1}^{N} \frac{(M_i - O_i)^2}{N} \right]^{1/2},$$

TABLE 2. Statistics of meteorological variables at CIT and some FLUXNET sites, including oak/pine forest, coastal sage, and grassland sites. Temperature and RH at 2 m and winds at 10 m above ground level are compared.

Site	Variable	Mean		RMSE	MB	IOA	N
		Model	Obs				
CIT	Temperature (°C)	18.8	17.7	1.7	1.0	0.96	768
	RH (%)	59.2	70.5	14.5	−11.2	0.84	768
	Wind speed; m s^{-1})	1.1	0.8	0.7	0.3	0.68	767
	SWDOWN (W m^{-2})	354.1	267.7	173.8	85.3	0.94	768
Oak/pine forest	Temperature (°C)	13.5	14.0	2.3	0.0	0.96	726
	RH (%)	53.6	47.0	17.0	4.6	0.83	726
	Wind speed (m s^{-1})	4.3	1.5	3.6	2.8	0.21	679
	SWDOWN (W m^{-2})	369.4.4	322.5	141.0	47.1	0.97	750
Coastal sage	Temperature (°C)	16.6	15.3	2.2	1.4	0.94	750
	RH (%)	70.7	70.7	10.8	−12.1	0.91	750
	Wind speed (m s^{-1})	1.9	1.6	1.0	0.4	0.67	750
	SWDOWN (W m^{-2})	338.7	287.2	158.3	55.3	0.96	750
Grassland	Temperature (°C)	17.4	14.8	3.3	2.6	0.86	750
	RH (%)	70.0	75.4	14.2	−5.1	0.85	750
	Wind speed (m s^{-1})	2.3	1.8	1.0	0.5	0.80	719
	SWDOWN (W m^{-2})	335.6	290.8	146.0	45.2	0.96	750

$$MB = \frac{\sum_{i=1}^{N}(M_i - O_i)}{N}, \quad \text{and}$$

$$IOA = 1 - \frac{\sum_{i=1}^{N}(M_i - O_i)^2}{\sum_{i=1}^{N}\left(\left|M_i - \frac{\sum_{i=1}^{N}O_i}{N}\right| + \left|O_i - \frac{\sum_{i=1}^{N}M_i}{N}\right|\right)^2}.$$

Here, M_i and O_i indicate modeling results and observations, respectively, at each grid point i.

a. Meteorological evaluation

The simulated meteorological results were compared with four ground measurements including CIT and three FLUXNET sites (Fig. 1), and their statistics are reported in Table 2. The modeling results captured day-to-day hourly variations of meteorological observations including 2-m temperature and relatively humidity (RH), 10-m winds, and surface SWDOWN at CIT (not shown). WRF-VPRM overestimated temperature by approximately 1.0°C, and the model underestimated RH by approximately 11%. The model overestimated wind speeds by approximately 0.3 m s^{-1}. Wind directions ranged from 120° to 240°: the south and southwest directions were dominant during day- and nighttime, respectively, which are associated with the Catalina eddies off the coast and the topography of Southern California, as described in section 1. Besides temperature, RH, and winds, the agreement of SWDOWN is also critical for calculating NEE. SWDOWN is very closely correlated

with photosynthesis active radiation (PAR); PAR ≈ 1.98 × SWDOWN (Mahadevan et al. 2008) and is used to compute GEE over vegetation areas. SWDOWN showed clear diurnal variations, starting from sunrise (0500 LST) and ending at sunset (1900 LST), with a midday peak around 1200 LST (not shown). Overall, the model overestimated SWDOWN by 85 W m^{-2} on average.

The volume of the PBL basically determines the concentration of species such as CO_2 and is fundamentally controlled by solar radiation, heating of the ground, and developing atmospheric turbulence within the PBL. The simulated PBLH started to increase around 0500 LST, reached a peak around 1200 LST, and then continually decreased until 2200–2300 LST. By comparing with the measured cloud-base heights, it was determined that the simulated PBLHs were over- and underestimated by approximately 56 and 128 m with IOAs of 0.68 and 0.55, respectively, during the day- and nighttime. Note that uncertainties may occur when directly comparing the simulated PBLHs with the cloud-base heights measured by the ceilometer, because 1) the model's coarser resolution often cannot resolve clouds that appear on the subgrid scale and can be detected by the ceilometer and 2) the simulated PBLH is sensitive to the model's PBL schemes, making it often hard to capture the measured PBLHs. To investigate the uncertainty of simulated PBLH, we estimated PBLH using the vertical profile of potential temperature measured by the NOAA P-3 aircraft during midday on 14, 16, and 19 May, when the aircraft flew spirals over CIT during daytime. The bias of modeled PBLH ranged approximately from 10 to 380 m (Fig. S2 in the online
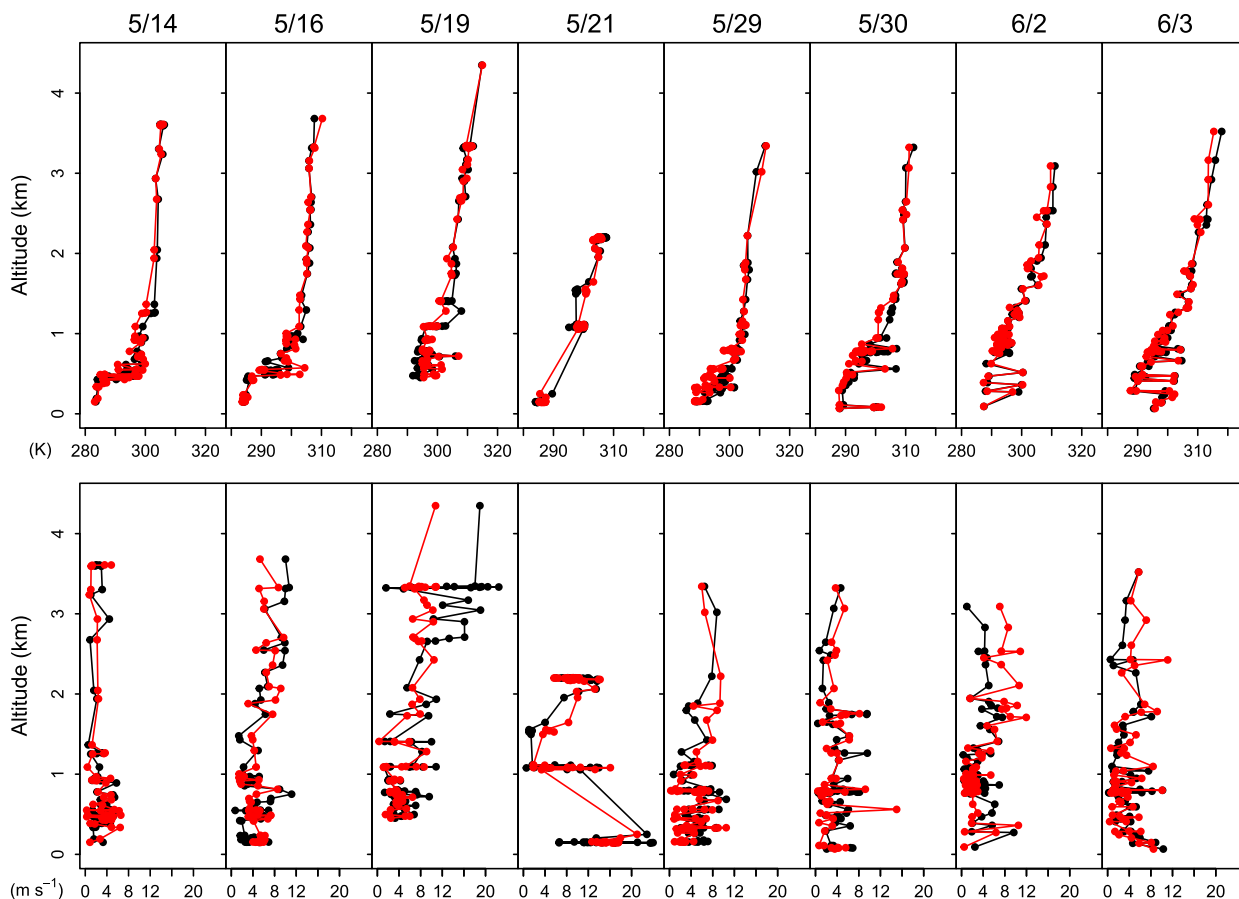
FIG. 2. Vertical profiles of (top) potential temperature and (bottom) wind speed for each of the eight flights during the study period. Red and black lines indicate WRF-VPRM results and NOAA P-3 aircraft observations, respectively.

supplemental material). This bias unfortunately cannot be directly compared with the ground ceilometer measurements because of the fact that there were no available measured values at the same time as the aircraft measurements.

The modeling results were also compared with NOAA P-3 aircraft observations. Among 18 days in total of the NOAA P-3 flights during CalNex 2010, we chose the days of 14, 16, 19, and 21 May for daytime and 29 and 30 May and 2 and 3 June for nighttime, when the aircraft flew over SoCAB. Each day's vertical profile of potential temperature and wind speed is displayed in Fig. 2. WRF-VPRM results showed good agreement with observed potential temperature along flight altitudes; they underestimated potential temperature by 0.1°C in daytime and overestimated by 1.4°C in nighttime. The model also captured the vertical wind profile, except at higher altitude (>3 km) on 19 May; it underestimated wind by $0.6 \, \mathrm{m \, s^{-1}}$ (IOA = 0.89; RMSE = $3.3 \, \mathrm{m \, s^{-1}}$) during daytime and $0.2 \, \mathrm{m \, s^{-1}}$ (IOA = 0.68; RMSE = $2.6 \, \mathrm{m \, s^{-1}}$) during nighttime.

b. CO_2 concentration

1) BACKGROUND CO_2 CONCENTRATIONS

To investigate the performance of the model's background CO_2 concentration, we used observational data measured at the Palos Verdes site (PV; 33°42′88″N, 118°18′70″W) in Fig. 1. This site is located at the southern end of SoCAB, on a steep hillside near the Pacific Ocean ~0.3 km above sea level, at which the concentrations of tracers transported by sea breezes to SoCAB can be monitored. Newman et al. (2013) measured CO_2 concentration and assumed the daily minimum hourly values at PV to be a constant background concentration of 393.1 ppm. We also assumed that the measured concentrations at this site can represent the "local" background concentration for SoCAB. Other CO_2 monitoring sites were not known to us during the study period. Our simulated result was close to the measured background concentration value with the offset of 0.1 ± 2.4 ppm.
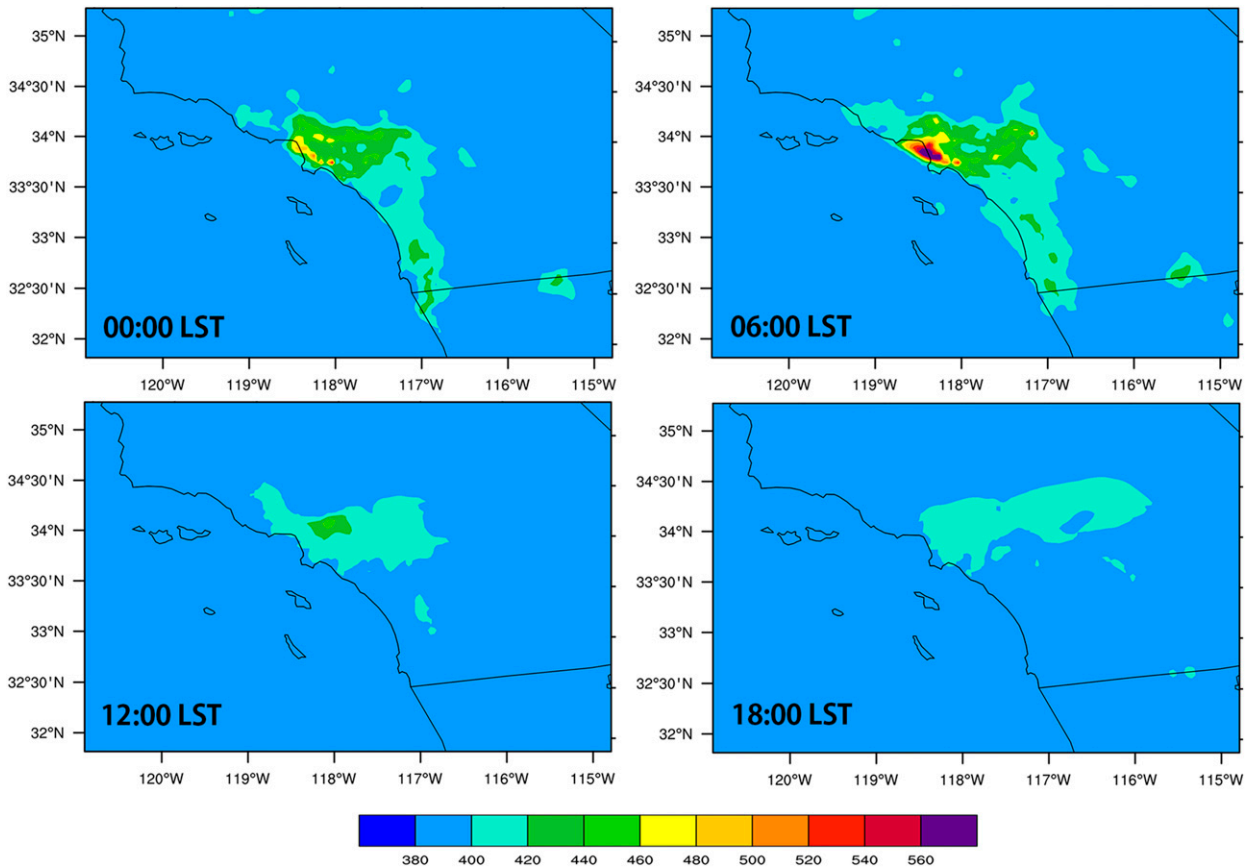
FIG. 3. Horizontal distribution of CO_2 concentrations (ppm) of the finest-scale domain (d03) on 21 May, displayed in 6-h intervals.

2) SPATIAL DISTRIBUTIONS

The horizontal and vertical distributions of CO_2 concentration are associated with the diurnal variation of the sea breeze, emissions, and PBLHs along with the topographical features of SoCAB—21 May was selected as an example of a typical day. Its diurnal pattern of CO_2 concentrations on horizontal and vertical cross-sectional distributions is displayed in Figs. 3 and 4, respectively. At 0600 LST in the early morning, the highest CO_2 concentration appeared to be due mainly to the combination of the smallest volume of PBL and the beginning of morning rush-hour vehicle CO_2 emissions. The heights of surrounding mountains are much higher than the average PBLH most of the time, preventing ventilation. Around 1200–1400 LST when the PBLH grew and the vegetation uptake increased, the sea breeze pushed the tracers over the mountains, and the concentration remained low until late afternoon (~1800 LST). After this time, CO_2 concentration started to increase again as a result of the evening rush-hour emissions along with the gradually decreasing PBLH and the increasing vegetation respiratory contribution, and high

concentrations were maintained through the night until early the next morning. This typical diurnal pattern of tracers for SoCAB agrees well with the results of other previous pollution studies (e.g., Chen et al. 2013).

3) COMPARISON WITH CIT GROUND OBSERVATIONS

The time series of the hourly variation of CO_2 concentration at CIT during the whole study period is shown in Fig. 5. WRF-VPRM captured the variation of CO_2 concentrations. The model overestimated by 9.2 ppm with IOA = 0.53 and RMSE = 17.0 ppm during daytime, and it overestimated by 1.6 ppm with IOA = 0.49 and RMSE = 1.8 ppm during nighttime.

To facilitate discussion of the variation of CO_2 concentrations together with emissions, the averaged diurnal variation of CO_2 emissions and concentrations at CIT and over SoCAB is displayed in Fig. 6, together with that of PBLHs. Over SoCAB, the anthropogenic CO_2 emissions increased during the morning rush hour (from 0500 to 0900 LST) and then increased again after 1300 LST until 1700 LST, showing a daily maximum
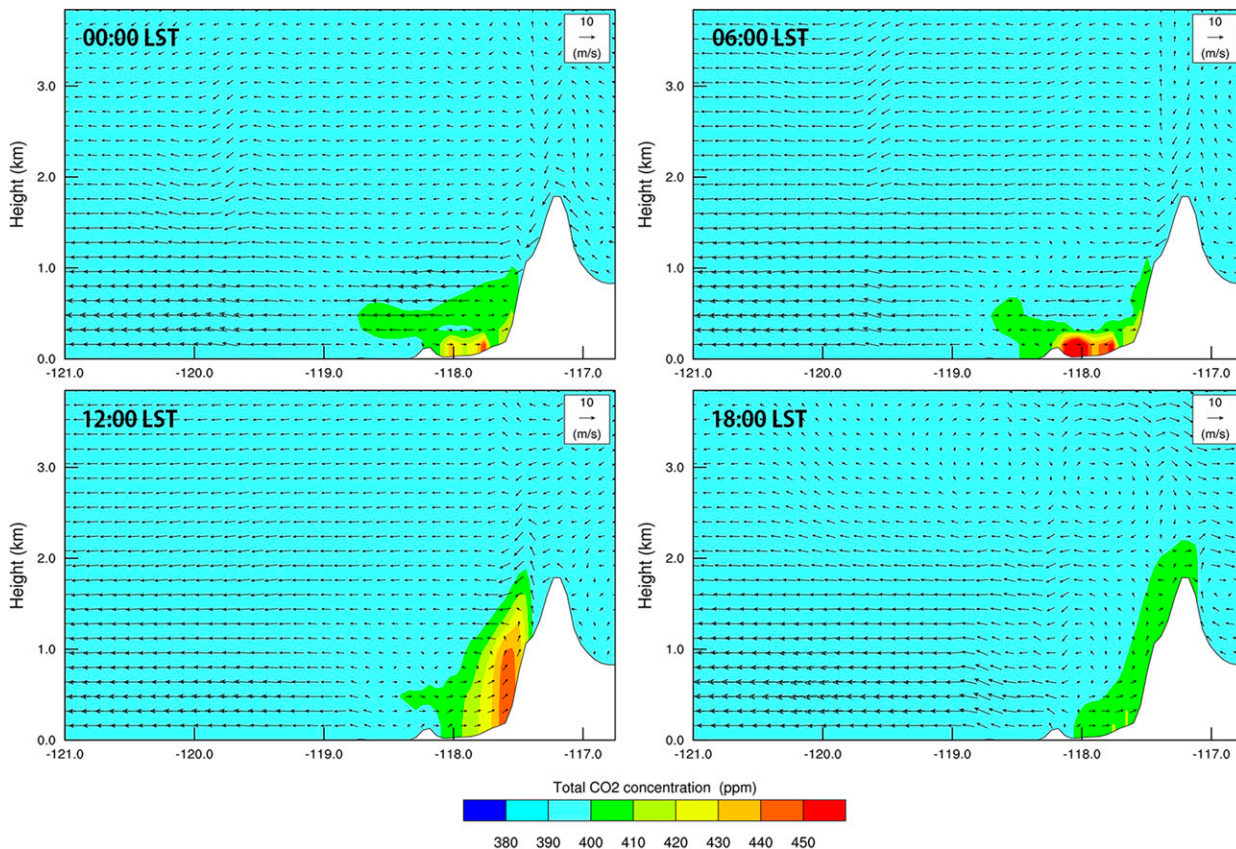
FIG. 4. Vertical cross section of CO_2 concentrations along the line indicated in Fig. 1 for 21 May, displayed in 6-h intervals.

peak. The larger second rush-hour peak was a typical emission pattern in metropolitan areas, such as in Houston, Texas (e.g., Park et al. 2010). The daytime emissions at CIT were about 2 times those averaged over SoCAB.

The averaged CO_2 concentrations at CIT were approximately 9 ppm higher than those over SoCAB, as expected. The CO_2 concentrations at CIT began to increase at 0500 LST and continued to rise until 0800 LST when the dominant morning rush hour ended, and values remained high until noon. In the afternoon, the concentrations decreased until 1600–1700 LST, associated with the highest PBLH and biospheric contribution, and then gradually increased again through the night until early the next morning as the PBLH decreased and the plant respiratory contribution increased.

During the early daytime (0600–1300 LST), WRF-VPRM overestimated the CO_2 concentrations
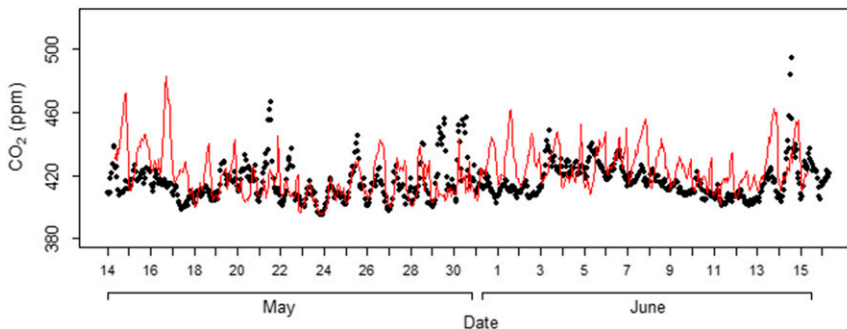

FIG. 5. Time series of CO_2 concentrations from simulations (red line) and ground observations (black dots) at CIT.
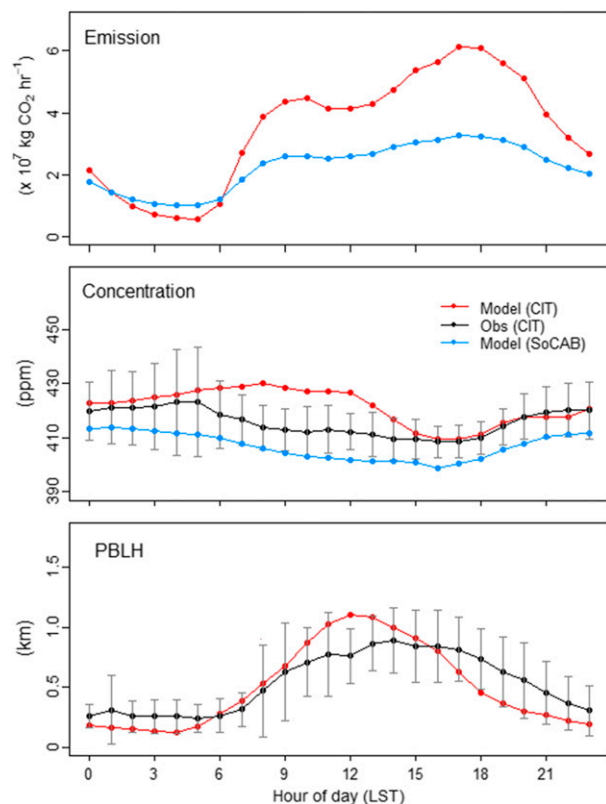
FIG. 6. Averaged diurnal variation of anthropogenic CO_2 emissions, concentrations, and PBLH at CIT and over SoCAB during the study period. Gray bars indicate 1 std dev for the observations.

by ~14 ppm on average (Fig. 6). The uncertainties of the model can be due to vertical mixing, advection, emissions, initial fields, and VPRM parameters, as described in previous studies (Ahmadov et al. 2007; Pillai et al. 2011). The overestimate of daytime CO_2 concentrations

may be caused by overestimates either of the first peak of emissions at CIT or of the advection from CO_2 source areas to CIT. To examine daytime emission sources affecting CIT by advection from specific wind directions, frequency of counts by wind direction of CO_2 concentration was compiled. The results are represented in Fig. 7. This exercise revealed that south and southwest, where downtown LA is located, were dominant daytime CO_2 source directions. The averaged simulated daytime CO_2 concentration in the dominant wind directions (150°–240°) was 421.8 ppm, which is comparable to the observed mean values of 411.9 ± 8.3 ppm. The Hestia emissions data used in this study are considered to be the "climatology" of emissions rather than the "weather" of emissions. This means that the emissions data would not represent "true" day-to-day hourly-basis variations in real environments. From the relatively low bias of the meteorological conditions, the uncertainties of emissions data in or around downtown LA may cause the overestimate of the simulated CO_2 concentrations during daytime. We still need comparisons at multiple measurement points for further investigation, however.

To extract anthropogenic and biospheric signals from the total CO_2 concentrations, two isotopic tracer radiocarbon ($\Delta^{14}C$) measurements were conducted at CIT during the study period by Newman et al. (2013), resulting in a finding that ~100% and ~50% of emissions were from fossil-fuel combustion during day- and nighttime, respectively. We compared the measured signals with "tagged" tracers built into WRF-VPRM, which can identify the contribution of different CO_2 sources between anthropogenic and biospheric signals (Ahmadov et al. 2009; Pillai et al. 2011). The simulated results showed positive values most of the time with a range of <2 ppm (Fig. S3 in the online supplemental
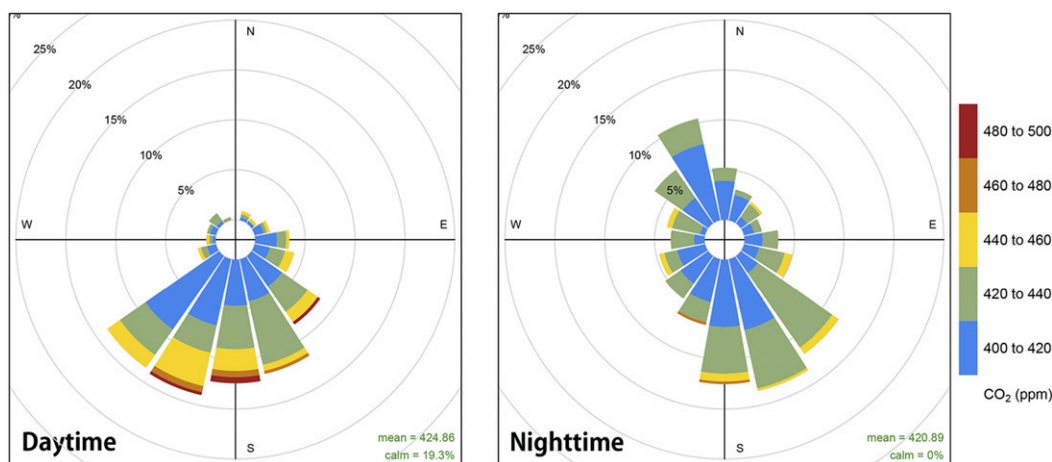

FIG. 7. Frequency of counts by wind direction (%) of simulated CO_2 concentration at CIT.
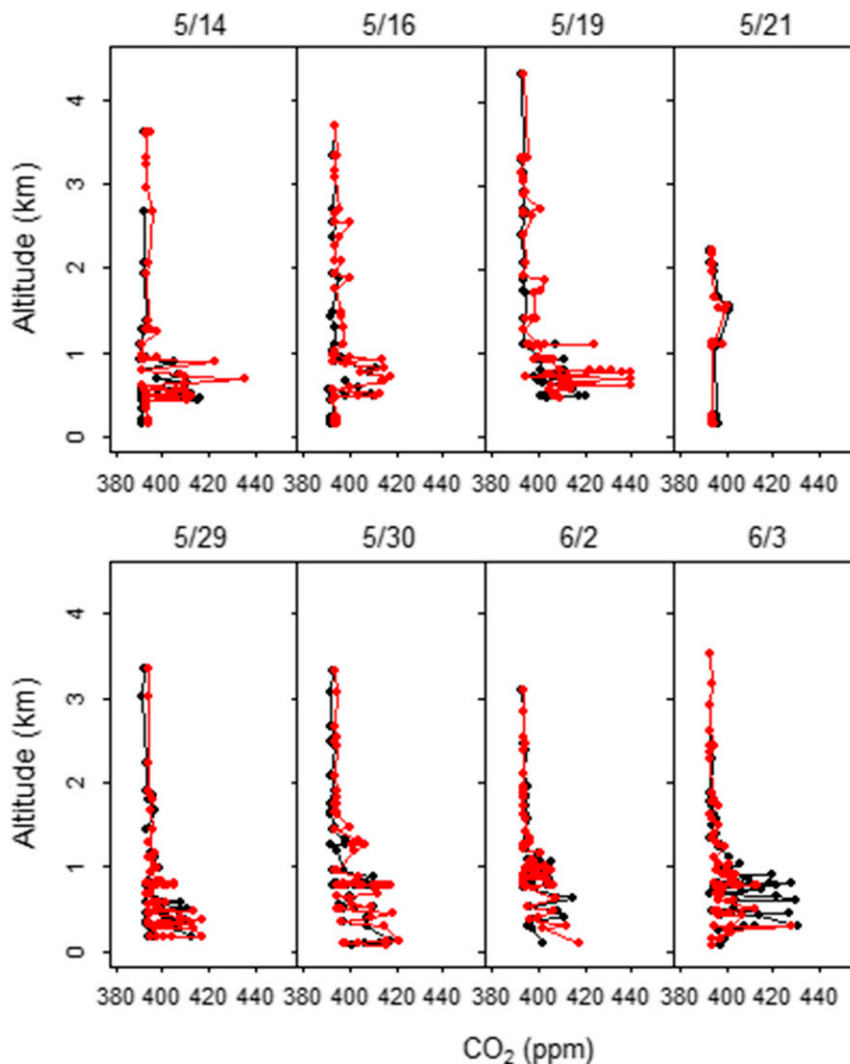
FIG. 8. As in Fig. 2, but for CO$_2$ concentrations.

material), which implied that our model successfully showed that the influence of fossil-fuel combustion was significant near CIT. Our model failed to capture the negative trend during the first half of the study period and underestimated the positive values by a factor of 3–5 during the second half period. This discrepancy may not be decreased simply by making model resolutions higher, as shown in the sensitivity tests in Feng et al. (2016). It seems that further investigation for both intensive measurements and improving models is needed in future studies.

4) Comparison with aircraft observations

Here, we discuss the comparison of the model results with aircraft observations, which was missing in the previous study of Feng et al. (2016). The observed and simulated CO$_2$ vertical profiles and time series for all eight flights are displayed in Figs. 8 and 9, respectively, and each flight's statistics are reported in Table 3. The model captured the vertical gradient of CO$_2$ concentrations, except at lower altitudes (<1 km) on 19 May and 3 June, on which days it significantly overestimated and underestimated the concentrations, respectively (Fig. 8). The relatively large discrepancies on the two noted days were not directly caused by the model's meteorological-simulation performance (Fig. 4). No clear correlation with wind directions was found (not shown).

The aircraft moved in and out of the PBL, flying over various land-cover types (Fig. 9). Overall, lower concentrations appeared over the ocean and above the PBL and higher concentrations occurred over the urban area and within the PBL. The model underestimated concentration by 1.8 ppm, with IOA = 0.81 and RMSE = 6.1 ppm, and by 0.3 ppm, with IOA = 0.74 and RMSE = 6.7 ppm,
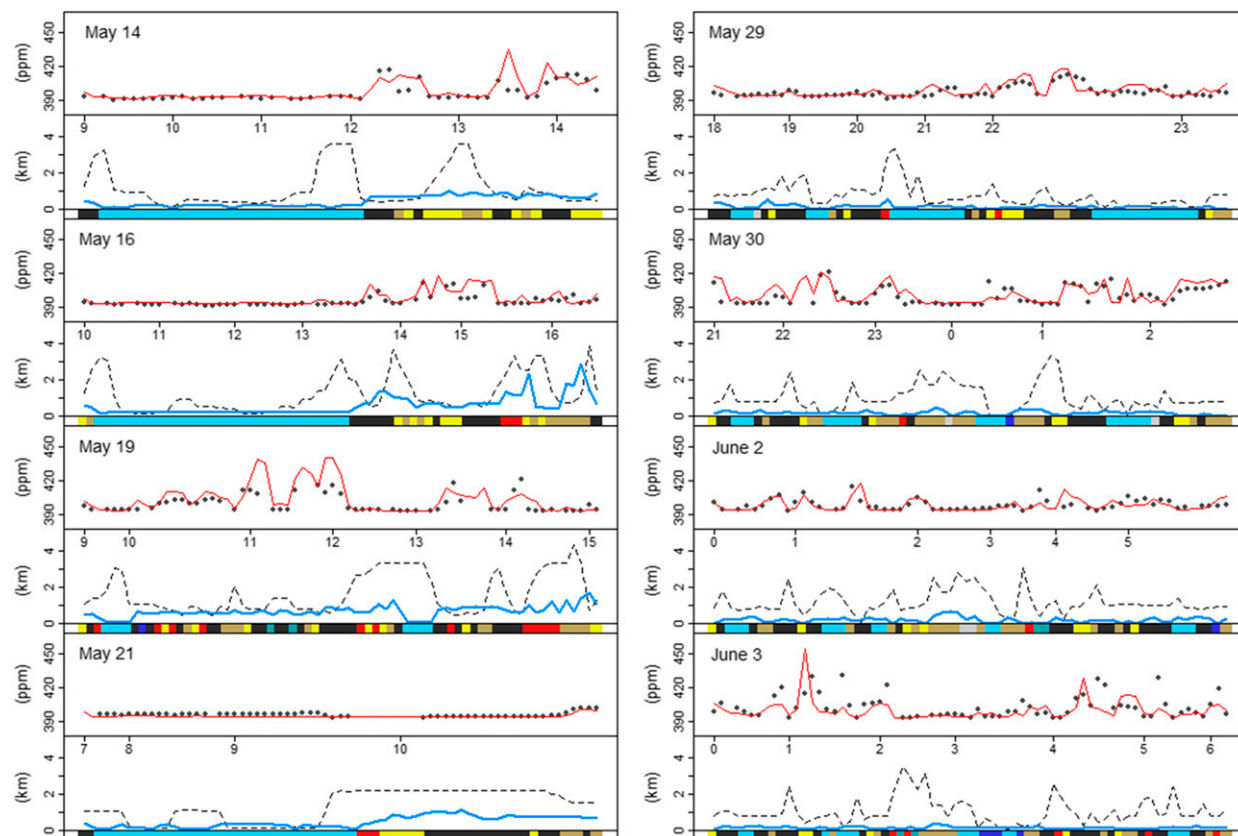
FIG. 9. Time series of CO_2 concentrations from simulations (red line) and aircraft observations (black dots), along with time series of aircraft altitudes (black dashed line) and simulated PBLHs (blue thick line). Land-cover types at the aircraft locations are represented by color codes as in Fig. 1.

during day- and nighttime flight days, respectively. During daytime, CO_2 concentrations within the PBL were ~7 ppm higher than those above the PBL, on average, without regard to land cover. The model's results showed a better agreement with observations above the PBLH, where there are fewer direct effects of heterogeneous emission sources. During nighttime, it appears that the aircraft moved above the nighttime PBL most of the time. High concentrations (>400 ppm) appeared at lower altitudes (<1 km) even above the nighttime PBLHs in both observations and simulations. This phenomenon could be due either to CO_2 concentrations in residual layers or to advection at high altitudes. For further investigations of the uncertainties at higher altitudes, inverse modeling as in the work of Brioude et al. (2013) can be used in future studies.

c. CO_2 fluxes

On the basis of the vegetation fraction retrieved by SYNMAP, the total vegetation area over SoCAB was estimated to be approximately 77%, mostly in the mountains, of which shrubland was the most dominant vegetation class (~62%) followed by evergreen forest (~33%), grassland (~4%), and savanna (~1%). To see by how much the simulated NEE was improved by optimization of VPRM parameters at each corresponding vegetation class site, we compared the averaged diurnal variations of simulated NEE and observed CO_2 flux, assuming that the simulated NEE is equal to the measured CO_2 flux. The results are displayed in Fig. 10. In comparing with the results from the prior VPRM parameters, it is seen that the statistics with posterior parameters were much improved.

Errors of simulated NEEs are likely attributed to the calculation of respiration by 2-m air temperature, as described by Ahmadov et al. (2009) and Pillai et al. (2011), and to the optimization approaches (Jamroensan 2013). In comparing with the results from prior VPRM parameters, it is seen that the model with the posterior parameters reduced the bias of simulated NEE by 40%, 48%, and 34% during daytime and 94%, 41%, and 26% during nighttime, at the oak/pine forest, coastal sage, and grassland sites, respectively. Note that the direct comparison of NEEs with fluxes of CO_2 measured by the

TABLE 3. Statistics for CO_2 concentrations between modeling results and aircraft observations.

Date	Mean		RMSE	MB	IOA	N
	Model	Obs				
14 May	398.3	396.1	7.5	2.6	0.78	48
16 May	397.0	394.6	4.5	1.9	0.80	61
19 May	397.0	398.9	4.5	1.9	0.80	61
21 May	394.6	395.5	1.5	−1.0	0.82	57
29 May	398.9	396.9	4.6	2.0	0.80	67
30 May	402.2	399.8	6.8	2.4	0.81	63
2 Jun	398.0	398.0	4.6	0.1	0.75	59
3 Jun	399.0	402.5	9.4	−3.3	0.61	65

eddy covariance method can naturally include uncertainties, because the fluxes include a CO_2 storage term within the canopy (Aubinet et al. 2012). In this study, however, we kept our assumption because of the facts that there is lack of storage-term information in FLUXNET data and that estimates of the storage term are outside the bounds of this study. Overall, the posterior VPRM parameters played an important role in improving the simulation results of NEE, and therefore we conclude that the optimization of VPRM parameters is essential for regional CO_2 modeling. Thus, the optimization can improve the estimate of the CO_2 budget over SoCAB (section 4d), in which multiple vegetation types are mixed.

d. Estimate of CO_2 budget

An estimate of the CO_2 budget is important for corrections to or updates of current environmental policy in relation to reductions in fossil-fuel carbon emissions that are mandated by California state law (Assembly Bill 32). In this section, we estimated the CO_2 budget over SoCAB during the CalNex 2010 period. Here we define the CO_2 budget over the whole area of SoCAB (Fig. 1) as the ratio of the total simulated NEEs to the total Hestia 2010 anthropogenic CO_2 emissions at all surface grid points. The amount of biospheric contribution was estimated at approximately −23% (daytime) and approximately +9% (nighttime) of the total anthropogenic CO_2 emissions during the study period. This vegetation contribution rate is higher than the value calculated with the prior VPRM parameters by approximately a factor of 2. Note that the study period was part of the vegetation growing season, and therefore a further long-term (~1 yr) simulation study, taking into account the seasonal leaf foliage, should be followed to assess the annual CO_2 budget.

During the process of optimization, another uncertainty from the VPRM parameters could emerge from a cutoff criterion of the u_* threshold value for the neighborhood-scale flux measurements. The u_* threshold value varies from site to site and from season to

season, and it is critical to filter underestimated measured CO_2 fluxes, especially during transition and nighttime. To evaluate the effects of the threshold value, we carried out sensitivity tests with additional cutoff criteria of $u_* < 0.2$ and $u_* < 0.0 \, \mathrm{m \, s}^{-1}$. These two values are widely used ranges in the micrometeorology literature. Results showed that the biospheric contribution relative to the anthropogenic emissions over SoCAB during the CalNex 2010 period is estimated to be in the range from −24% to −20% during daytime and from +8% to +9% during nighttime, in consideration of the uncertainty from cutoff criteria. On the basis of the land-cover distribution, it appears that the biospheric CO_2 uptake mainly occurred in the vegetation-dominated mountain regions in SoCAB.

5. Summary and conclusions

In this study, a coupled WRF-VPRM model was applied over the anthropogenic-CO_2-emission-rich region of SoCAB during the CalNex 2010 period, in contrast to most previous studies, which were mainly focused on vegetation-dominated areas. Discriminating from a similar previous study of Feng et al. (2016), here 1) VPRM parameters were optimized for better performance of the biospheric module and 2) the newly updated version of Hestia-LA combined with the FFDAS anthropogenic CO_2 emission data and the CT2015 CO_2 mole-fraction data was used. We reported the performance of WRF-VPRM for CO_2 transport and temporal variability in comparison with the observations and also discussed the model's improvement from the VPRM parameter optimization. Last, we presented the estimated CO_2 budget over SoCAB.

The WRF-VPRM successfully recreated the meteorological variables for both ground- and aircraft-based measurements. The model also captured the diurnal variation of CO_2 concentrations at the ground sites but slightly overestimated daytime CO_2 concentrations. The analysis of daytime CO_2 concentrations by wind direction implied that the uncertainty of local emission sources located in the south and southwest directions, where downtown LA is located, affected the model overestimation of CO_2 concentrations at the ground measurement site. The model also matched the vertical profile and times series of CO_2 concentrations, in comparison with the NOAA P-3 aircraft measurements, but the modeled CO_2 concentrations were over- and underestimated at lower altitudes on 19 May and 3 June, respectively.

After validating the improvement of NEE calculation with posterior VPRM parameters, the total biospheric contribution rate was calculated over SoCAB, resulting
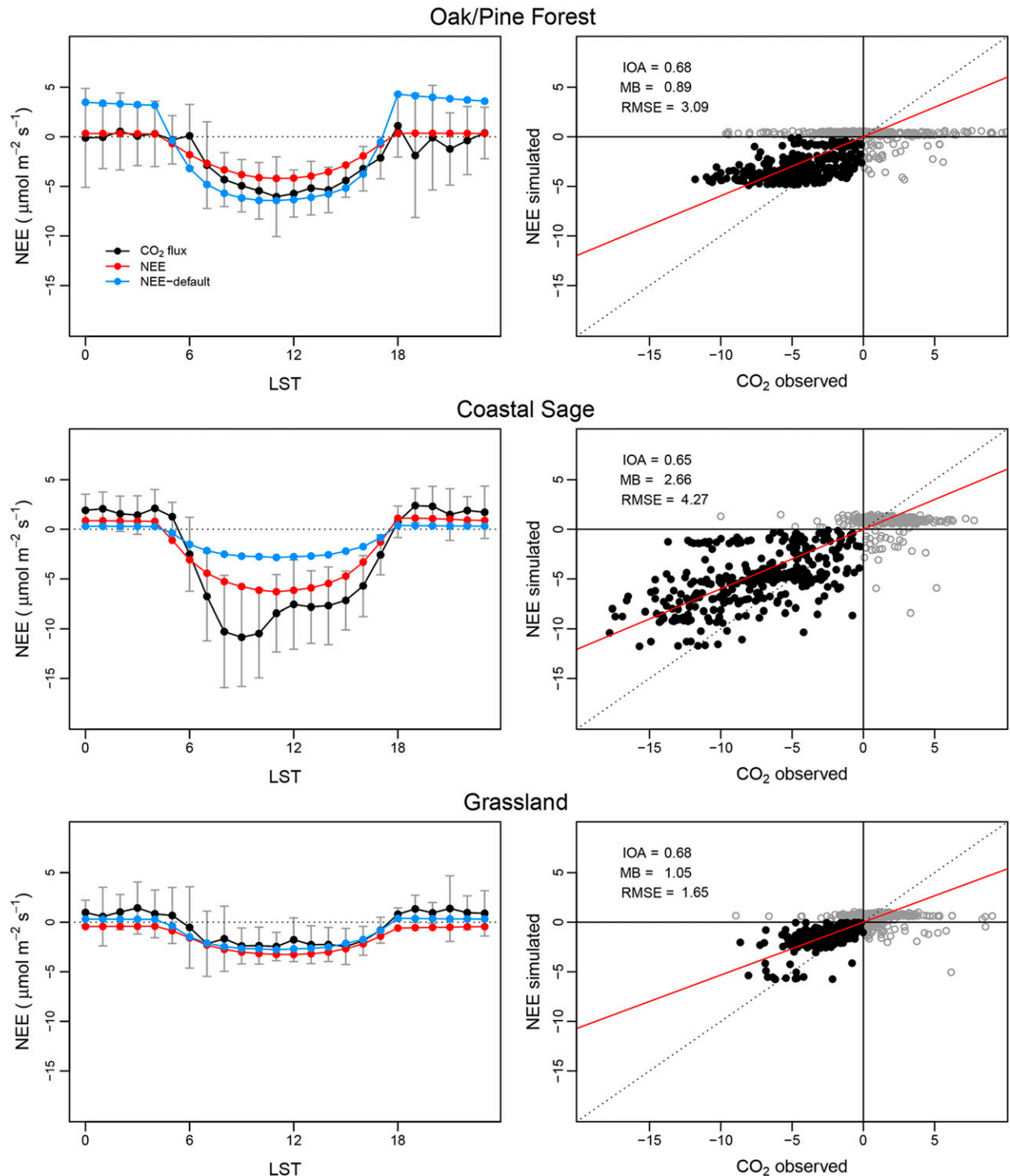
FIG. 10. Averaged diurnal variation and scatterplots of simulated NEEs and observed CO_2 fluxes at three FLUXNET sites, including oak/pine forest, coastal sage, and grassland. NEE and ''NEE-default'' are the simulated result with posterior and prior VPRM parameters, respectively. The black dashed line indicates a 1-to-1 line, and the red line indicates the linear-regression line for daytime only (black dots). Nighttime data (gray circles) are excluded from statistics.

in a range from −24% to −20% (in daytime) and from +8% to +9% (in nighttime) of the total anthropogenic CO_2 emissions. The uncertainty of the CO_2 budget was reduced by approximately a factor of 2 relative to the results from the prior VPRM parameters. Overall, SoCAB played a role as a net emission source of CO_2 during the study period.

The output of this modeling study can be used to validate remote sensing instruments and as the priori for regional inverse modeling, as well as to support environmental policy in relation not only to emission control of fossil-fuel carbon but also to vegetation management in the state of California. As the first goal of the study, the slant column concentration of CO_2, the total number of absorbing molecules per unit area along the sun–Earth–instrument optical path, over LA can also be compared with and used to calibrate the California Laboratory for Atmospheric Remote Sensing facility currently set up on Mount Wilson for the continuous monitoring of air pollution and greenhouse gases in SoCAB (Wong et al. 2015). The study's total column concentrations from WRF-VPRM results can be compared with data from the *Orbiting Carbon Observatory-2* (*OCO-2*; Eldering et al. 2017) or the Japanese *Greenhouse Gas Observing Satellite* (*GOSAT*), as in the work of Hedelius et al. (2017).

REFERENCES

Ahmadov, R., C. Gerbig, R. Kretschmer, S. Koerner, B. Neininger, A. J. Dolman, and C. Sarrat, 2007: Mesoscale covariance of transport and CO_2 fluxes: Evidence from observations and simulations using the WRF-VPRM coupled atmosphere–biosphere model. *J. Geophys. Res.*, **112**, D22107, https://doi.org/10.1029/2007JD008552.

——, ——, ——, S. Korner, C. Rodenbeck, P. Bousquet, and M. Ramonet, 2009: Comparing high resolution WRF-VPRM simulations and two global CO_2 transport models with coastal tower measurements of CO_2. *Biogeosciences*, **6**, 807–817, https://doi.org/10.5194/bg-6-807-2009.

Angevine, W. M., L. Eddington, K. Durkee, C. Fairall, L. Bianco, and J. Brioude, 2012: Meteorological model evaluation for CalNex 2010. *Mon. Wea. Rev.*, **140**, 3885–3906, https://doi.org/10.1175/MWR-D-12-00042.1.

Asefi-Najafabady, S., and Coauthors, 2014: A multiyear, global gridded fossil fuel CO_2 emission data product: Evaluation and analysis of results. *J. Geophys. Res. Atmos.*, **119**, 10 213–10 231, https://doi.org/10.1002/2013JD021296.

Aubinet, M., C. Feigenwinter, B. Heinesch, Q. Laffineur, D. Papale, M. Reichstein, J. Rinne, and E. Van Gorsel, 2012: Nighttime flux correlation. *Eddy Covariance: A Practical Guide to Measurement and Data Analysis*, M. Aubinet, T. Vesala, and D. Papale, Eds., Springer, 133–157.

Auch, R., J. Taylor, and W. Acevedo, 2004: Urban growth in American cities: Glimpses of U.S. urbanization. U.S. Geological Survey Circular 1252, 52 pp., https://pubs.er.usgs.gov/publication/cir1252.

Baldocchi, D., and Coauthors, 2001: FLUXNET: A new tool to study the temporal and spatial variability of ecosystem-scale carbon dioxide, water vapor, and energy flux densities. *Bull. Amer. Meteor. Soc.*, **82**, 2415–2434, https://doi.org/10.1175/1520-0477(2001)082<2415:FANTTS>2.3.CO;2.

Belward, A. S., J. E. Estes, and K. D. Kline, 1999: The IGBP-DIS global 1-km land-cover data set DISCover: A project overview. *Photogramm. Eng. Remote Sensing*, **65**, 1013–1020.

Bernardet, L., and Coauthors, 2008: The Developmental Testbed Center and its winter forecasting experiment. *Bull. Amer. Meteor. Soc.*, **89**, 611–628, https://doi.org/10.1175/BAMS-89-5-611.

Bowden, R. D., K. J. Nadelhoffer, R. D. Boone, J. M. Melillo, and J. B. Garrison, 1993: Contributions of aboveground litter, belowground litter, and root respiration to total soil respiration in a temperate mixed hardwood forest. *Can. J. For. Res.*, **23**, 1402–1407, https://doi.org/10.1139/x93-177.

Brioude, J., and Coauthors, 2013: Top-down estimate of surface flux in the Los Angeles Basin using a mesoscale inverse modeling technique: Assessing anthropogenic emissions of CO, NO_x and CO_2 and their impacts. *Atmos. Chem. Phys.*, **13**, 3661–3677, https://doi.org/10.5194/acp-13-3661-2013.

Chen, D., and Coauthors, 2013: WRF-Chem simulation of NO_x and O_3 in the L.A. basin during CalNex-2010. *Atmos. Environ.*, **81**, 421–432, https://doi.org/10.1016/j.atmosenv.2013.08.064.

Conil, S., and A. Hall, 2006: Local regimes of atmospheric variability: A case study of Southern California. *J. Climate*, **19**, 4308–4325, https://doi.org/10.1175/JCLI3837.1.

Eldering, A., and Coauthors, 2017: The *Orbiting Carbon Observatory-2*: First 18 months of science data products. *Atmos. Meas. Tech.*, **10**, 549–563, https://doi.org/10.5194/amt-10-549-2017.

Feng, S., and Coauthors, 2016: Los Angeles megacity: A high-resolution land–atmosphere modelling system for urban CO_2 emissions. *Atmos. Chem. Phys.*, **16**, 9019–9045, https://doi.org/10.5194/acp-16-9019-2016.

Forster, P., and Coauthors, 2007: Changes in atmospheric constituents and in radiative forcing. *Climate Change 2007: The Physical Science Basis*, S. Solomon et al., Eds., Cambridge University Press, 129–234.

Gerbig, C., J. C. Lin, S. C. Wofsy, B. C. Daube, A. E. Andrews, B. B. Stephens, P. S. Bakwin, and C. A. Grainger, 2003: Toward constraining regional-scale fluxes of CO_2 with atmospheric observations over a continent: 2. Analysis of COBRA data using a receptor-oriented framework. *J. Geophys. Res.*, **108**, 4757, https://doi.org/10.1029/2003JD003770.

Gurney, K. R., D. L. Mendoza, Y. Y. Zhou, M. L. Fischer, C. C. Miller, S. Geethakumar, and S. de la Rue du Can, 2009: High resolution fossil fuel combustion CO_2 emission fluxes for the United States. *Environ. Sci. Technol.*, **43**, 5535–5541, https://doi.org/10.1021/es900806c.

——, I. Razlivanov, Y. Song, Y. Y. Zhou, B. Benes, and M. Abdul-Massih, 2012: Quantification of fossil fuel CO_2 emissions on the building/street scale for a large U.S. city. *Environ. Sci. Technol.*, **46**, 12 194–12 202, https://doi.org/10.1021/es3011282.

Haman, C. L., B. Lefer, and G. A. Morris, 2012: Seasonal variability in the diurnal evolution of the boundary layer in a near-coastal urban environment. *J. Atmos. Oceanic Technol.*, **29**, 697–710, https://doi.org/10.1175/JTECH-D-11-00114.1.

Hedelius, J. K., and Coauthors, 2017: Emissions and topographic effects on column CO2 (X_{CO_2}) variations, with a focus on the Southern California megacity. *J. Geophys. Res. Atmos.*, **122**, 7200–7215, https://doi.org/10.1002/2017JD026455.

Hong, S. Y., Y. Noh, and J. Dudhia, 2006: A new vertical diffusion package with an explicit treatment of entrainment processes. *Mon. Wea. Rev.*, **134**, 2318–2341, https://doi.org/10.1175/MWR3199.1.

IPCC, 2013: *Climate Change 2013: The Physical Science Basis.* Cambridge University Press, 1535 pp., https://doi.org/10.1017/CBO9781107415324.

Jamroensan, A., 2013: Improving bottom-up and top-down estimates of carbon fluxes in the midwestern USA. Ph.D. thesis, University of Iowa, 121 pp., http://ir.uiowa.edu/etd/2530/.

Jimenez, P. A., and J. Dudhia, 2012: Improving the representation of resolved and unresolved topographic effects on surface wind in the WRF Model. *J. Appl. Meteor. Climatol.*, **51**, 300–316, https://doi.org/10.1175/JAMC-D-11-084.1.

Jung, M., K. Henkel, M. Herold, and G. Churkina, 2006: Exploiting synergies of global land cover products for carbon cycle modeling. *Remote Sens. Environ.*, **101**, 534–553, https://doi.org/10.1016/j.rse.2006.01.020.

Kotthaus, S., and C. S. B. Grimmond, 2012: Identification of microscale anthropogenic CO_2, heat and moisture sources—Processing eddy covariance fluxes for a dense urban environment. *Atmos. Environ.*, **57**, 301–316, https://doi.org/10.1016/j.atmosenv.2012.04.024.

Le Quere, C., and Coauthors, 2014: Global carbon budget 2013. *Earth Syst. Sci. Data*, **6**, 235–263, https://doi.org/10.5194/essd-6-235-2014.

Mahadevan, P., and Coauthors, 2008: A satellite-based biosphere parameterization for net ecosystem CO_2 exchange: Vegetation Photosynthesis and Respiration Model (VPRM). *Global Biogeochem. Cycles*, **22**, GB2005, https://doi.org/10.1029/2006GB002735.

Mesinger, F., and Coauthors, 2006: North American Regional Reanalysis. *Bull. Amer. Meteor. Soc.*, **87**, 343–360, https://doi.org/10.1175/BAMS-87-3-343.

Newman, S., and Coauthors, 2013: Diurnal tracking of anthropogenic CO_2 emissions in the Los Angeles basin megacity during spring 2010. *Atmos. Chem. Phys.*, **13**, 4359–4372, https://doi.org/10.5194/acp-13-4359-2013.

National Research Council, 2010: *Advancing the Science of Climate Change.* The National Academies Press, 526 pp.

Park, C., and G. W. Schade, 2016: Anthropogenic and biogenic features of long-term measured CO_2 flux in north downtown Houston, Texas. *J. Environ. Qual.*, **45**, 253–265, https://doi.org/10.2134/jeq2015.02.0115.

——, ——, and I. Boedeker, 2010: Flux measurements of volatile organic compounds by the relaxed eddy accumulation method combined with a GC-FID system in urban Houston, Texas. *Atmos. Environ.*, **44**, 2605–2614, https://doi.org/10.1016/j.atmosenv.2010.04.016.

Peischl, J., and Coauthors, 2012: Airborne observations of methane emissions from rice cultivation in the Sacramento Valley of California. *J. Geophys. Res.*, **117**, D00V25, https://doi.org/10.1029/2012JD017994.

Pérez-Landa, G., and Coauthors, 2007: Mesoscale circulations over complex terrain in the Valencia coastal region,

Spain—Part 2: Modeling CO_2 transport using idealized surface fluxes. *Atmos. Chem. Phys.*, **7**, 1851–1868, https://doi.org/10.5194/acp-7-1851-2007.

Peters, W., and Coauthors, 2007: An atmospheric perspective on North American carbon dioxide exchange: CarbonTracker. *Proc. Natl. Acad. Sci. USA*, **104**, 18 925–18 930, https://doi.org/10.1073/pnas.0708986104.

Petrescu, A. M. R., R. Abad-Vinas, G. Janssens-Maenhout, V. N. B. Blujdea, and G. Grassi, 2012: Global estimates of carbon stock changes in living forest biomass: EDGARv4.3—Time series from 1990 to 2010. *Biogeosciences*, **9**, 3437–3447, https://doi.org/10.5194/bg-9-3437-2012.

Peylin, P., and Coauthors, 2005: Daily CO_2 flux estimates over Europe from continuous atmospheric measurements: 1, inverse methodology. *Atmos. Chem. Phys.*, **5**, 3173–3186, https://doi.org/10.5194/acp-5-3173-2005.

Pillai, D., and Coauthors, 2011: High-resolution simulations of atmospheric CO_2 over complex terrain—Representing the Ochsenkopf mountain tall tower. *Atmos. Chem. Phys.*, **11**, 7445–7464, https://doi.org/10.5194/acp-11-7445-2011.

Ryan, M. G., and B. E. Law, 2005: Interpreting, measuring, and modeling soil respiration. *Biogeochemistry*, **73**, 3–27, https://doi.org/10.1007/s10533-004-5167-7.

Ryerson, T. B., and Coauthors, 2013: The 2010 California Research at the Nexus of Air Quality and Climate Change (CalNex) field study. *J. Geophys. Res.*, **118**, 5830–5866, https://doi.org/10.1002/jgrd.50331.

Satterthwaite, D., 2008: Cities' contribution to global warming: Notes on the allocation of greenhouse gas emissions. *Environ. Urbanization*, **20**, 539–549, https://doi.org/10.1177/0956247808096127.

Seto, K. C., and Coauthors, 2014: Human settlements, infrastructure and spatial planning. *Climate Change 2014: Mitigation of Climate Change*, O. Edenhofer et al., Eds., Cambridge University Press, 923–1000.

Tans, P. P., I. Y. Fung, and T. Takahashi, 1990: Observational constraints on the global atmospheric CO_2 budget. *Science*, **247**, 1431–1438, https://doi.org/10.1126/science.247.4949.1431.

Turnbull, J. C., and Coauthors, 2011: Assessment of fossil fuel carbon dioxide and other anthropogenic trace gas emissions from airborne measurements over Sacramento, California in spring 2009. *Atmos. Chem. Phys.*, **11**, 705–721, https://doi.org/10.5194/acp-11-705-2011.

Ulrickson, B. L., and C. F. Mass, 1990: Numerical investigation of mesoscale circulations over the Los Angeles Basin. Part I: A verification study. *Mon. Wea. Rev.*, **118**, 2138–2161, https://doi.org/10.1175/1520-0493(1990)118<2138:NIOMCO>2.0.CO;2.

van der Molen, M. K., and A. J. Dolman, 2007: Regional carbon fluxes and the effect of topography on the variability of atmospheric CO_2. *J. Geophys. Res.*, **112**, D01104, https://doi.org/10.1029/2006JD007649.

Velasco, E., M. Roth, S. H. Tan, M. Quak, S. D. A. Nabarro, and L. Norford, 2013: The role of vegetation in the CO_2 flux from a tropical urban neighbourhood. *Atmos. Chem. Phys.*, **13**, 10 185–10 202, https://doi.org/10.5194/acp-13-10185-2013.

Willmott, C. J., 1982: Some comments on the evaluation of model performance. *Bull. Amer. Meteor. Soc.*, **63**, 1309–1313, https://doi.org/10.1175/1520-0477(1982)063<1309:SCOTEO>2.0.CO;2.

Wong, K. W., and Coauthors, 2015: Mapping $CH_4 : CO_2$ ratios in Los Angeles with CLARS-FTS from Mount Wilson, California. *Atmos. Chem. Phys.*, **15**, 241–252, https://doi.org/10.5194/acp-15-241-2015.